NJC

PAPER

View Article Online
View Journal | View Issue

Cite this: *New J. Chem.*, 2026, **50**, 471

Binding thermodynamics of (*E*)-2-((2-hydroxybenzylidene)amino)-5-methylbenzonitrile and (*E*)-2-((2-hydroxybenzylidene)amino)-5-methylbenzonitrile cobalt(II) with HSA: an experimental and molecular dynamic study

Sheldon Sookai, *[a] Ibrahim Waziri,[b] Alfred J. Muller[b] and Monika Nowakowska*[a]

The interaction of small-molecule ligands with human serum albumin (HSA) critically influences drug bioavailability and pharmacokinetics. This study examines the binding characteristics of the free ligand **HL** and its cobalt(II) complex, **CoL**, using spectroscopic techniques, molecular docking, and molecular dynamics (MD) simulations. Fluorescence quenching assays confirm a dose-dependent interaction *via* a dynamic quenching mechanism, with **HL** exhibiting a 1.8-fold higher binding affinity at 310 K ($\log K_a$ = 5.13) than **CoL** ($\log K_a$ = 4.90), indicating reduced protein interaction upon metal complexation. Thermodynamic analyses reveal ΔH and ΔS values for **HL** and **CoL** to be 16.34, 10.36 kJ mol^{-1} and 0.15, 0.13 J K^{-1} mol^{-1}, respectively, indicating an entropy-driven binding process, with **HL** demonstrating greater entropic contribution. Circular dichroism spectroscopy (UV-CD) shows minimal secondary structure perturbation, though **CoL** induces a slight reduction in α-helicity. Near-UV CD shifts and *in silico* docking confirm preferential binding at Sudlow's site I, near Trp-214, supporting fluorescence data. Furthermore, site displacement assays suggest possible multi-site binding for both **CoL** and **HL**. Experimental data was well supported by MD simulations over a 100 ns trajectory. These findings suggest **HL**'s stronger HSA affinity could influence its bioavailability, whereas **CoL** exhibits reduced binding due to steric and electronic effects of metal coordination. This study enhances understanding of protein–ligand interactions, informing rational drug design strategies for albumin-bound therapeutics.

Received 9th September 2025,
Accepted 4th December 2025

DOI: 10.1039/d5nj03624k

rsc.li/njc

Introduction

The discovery of cisplatin revolutionized bioinorganic chemistry, establishing metal-based therapeutics as a cornerstone of modern cancer treatment. Today, nearly half of all cancer patients undergo chemotherapy with platinum-based drugs;[1] however, their clinical utility is often compromised by dose-limiting toxicity, poor tumour selectivity, and the emergence of intrinsic or acquired resistance, necessitating the search for next-generation metallodrugs with improved pharmacological profiles.[2,3] A promising approach to overcoming these limitations involves the development of transition-metal complexes that achieve an optimal balance between maximal antitumour potency and minimal systemic toxicity.[4] Researchers have increasingly investigated non-platinum alternatives, exploring compounds incorporating gold(III),[5,6] palladium(II),[7] ruthenium(II),[8] iridium(III),[9] copper(II),[10,11] nickel(II),[12] and cobalt(II/III),[13,14] many of which have demonstrated superior cytotoxic activity compared to cisplatin. Transition metals possess unique biochemical properties, including variable oxidation states, diverse coordination geometries, and tuneable ligand-binding capabilities, making them ideal candidates for rational drug design. Among these metals, cobalt stands out as a promising yet relatively underexplored alternative in cancer chemotherapy.

As an essential trace element, cobalt plays a fundamental role in biological processes through its incorporation in vitamin B_{12}.[15] Given its biocompatibility and ability to form stable complexes, cobalt-based therapeutics hold promise for anticancer drug development.[4] Notably, *in vitro* studies demonstrated that cobalt complexes exhibit potent anticancer activity,[16] particularly against MCF-7, A431, and HeLa cancer cell lines, exhibiting greater cytotoxic efficiency than cisplatin.[17–19] To date, Doxovir[20] remains the only cobalt(III) Schiff base complex to reach clinical trials,

[a] *Molecular Sciences Institute, School of Chemistry, University of the Witwatersrand, Private Bag X3, P.O. WITS 2050, Johannesburg, South Africa. E-mail: Sheldon.Sookai@wits.ac.za, Monika.Nowakowska@wits.ac.za; Web: https://www.wits.ac.za/chemistry/; Tel: +27 11 717-6727*
[b] *Research Centre for Synthesis and Catalysis, Department of Chemical Sciences, University of Johannesburg, Johannesburg, South Africa*

where it has shown efficacy against drug-resistant herpes simplex virus 1. This highlights the need for further development of novel cobalt-Schiff base therapeutics. Schiff bases are integral to bioinorganic and medicinal chemistry research due to their ease of synthesis, high coordination flexibility, and diverse bioactivity.[21,22] These ligands readily coordinate with a variety of transition metals,[23] yielding metal complexes with antioxidative,[24] anticancer,[25] antimicrobial,[26] and antiviral effects, including potential anti-COVID properties.[27] Among Schiff base frameworks, salicylaldehyde-derived Schiff bases have garnered significant interest, given their synthetic accessibility, stability, and efficacy in anticancer applications.[23,28,29] Recent work by Waziri *et al.*[30] demonstrated that a cobalt(II) Schiff base complex derived from (*E*)-2-((2-hydroxybenzylidene)amino)-5-methylbenzonitrile (**CoL**) exhibited exceptional cytotoxicity against MCF-7 cells ($IC_{50} < 5$ μM), outperforming doxorubicin ($IC_{50} < 48.03$ μM), a widely used clinical therapeutic. Its potent anticancer activity was attributed to DNA intercalation and apoptosis induction. While these findings highlight the therapeutic promise of cobalt-Schiff base complexes, a critical knowledge gap remains how metal coordination influences pharmacokinetics through serum protein binding. Building upon Waziri *et al.*'s work, this study aims to evaluate the binding interactions of **CoL** with human serum albumin (HSA), the predominant transport protein in the circulatory system.[30] As a key determinant of drug bioavailability, HSA plays a crucial role in modulating pharmacokinetics, distribution, and therapeutic efficacy by reversibly binding a broad spectrum of pharmaceutical compounds at primary drug binding regions, Sudlow's sites I and II,[31,32] Approved albumin-bound formulations such as Abraxane[33] have demonstrated the viability of HSA as a drug delivery system, improving the pharmacological performance of chemotherapeutics like paclitaxel,[33] docetaxel, and doxorubicin.[34] Despite extensive studies on platinum drugs and small molecules, systematic investigations of cobalt-Schiff base complexes with HSA remain scarce. Understanding the **CoL**–HSA interaction is therefore critical in assessing its potential for enhanced therapeutic precision.

This study addresses this gap by providing a comprehensive, multi-level analysis of HSA interactions with a salicylaldehyde-derived Schiff base ligand, (*E*)-2-((2-hydroxybenzylidene)amino)-5-methylbenzonitrile (**HL**), and its cobalt(II) complex (**CoL**). Unlike prior work that primarily focused on cytotoxicity or static docking, we combine fluorescence spectroscopy, UV-CD, molecular docking, and long-timescale molecular dynamics (MDS) to elucidate binding mechanisms, thermodynamic drivers, and structural stability under physiological conditions. Molecular docking predicts preferred ligand orientations and binding affinities within protein sites, rapidly identifying key atomic-level interactions, while MDS extends these insights by modeling the temporal evolution of protein–ligand complexes, capturing conformational flexibility, solvent effects, and dynamic stability beyond static models. By integrating experimental and computational approaches, recently recognized as powerful tools for rational drug design,[35–37] this work advances the understanding of protein–metallodrug interactions and informs design principles for albumin-bound cobalt therapeutics, with broader implications for anticancer, antiviral, and protein-engineering applications.

Synthesis of HL and CoL

The Co(II) chelate, **CoL**, was synthesized following the procedure outlined in Scheme 1. The Schiff base ligand, (*E*)-2-((2-hydroxybenzylidene)amino)-5-methylbenzonitrile (**HL**), was prepared *via* a condensation reaction between 2-hydroxybenzaldehyde and 2-amino-5-methylbenzonitrile. Complexation of the ligand with cobalt(II) acetate tetrahydrate in a 2 : 1 ligand-to-metal molar ratio, using a dichloromethane–methanol solvent mixture, afforded the **CoL** complex. The product precipitated as a solid and was isolated in good yield (65–76%). Both the ligand and the complex were characterized using standard spectroscopic and analytical techniques (see SI Fig. S1–S12).

The ^{1}H and ^{13}C NMR spectra of the Schiff base ligand **HL** (SI Fig. S1 and S2) exhibit characteristic signals consistent with its proposed structure. The hydroxyl proton (–OH) appears as a singlet at δ 12.46 ppm,[38] indicative of intramolecular hydrogen bonding. The imine proton (–CH═N) also resonates as a singlet at δ 9.10 ppm, which is notably downfield compared to values typically reported for salicylaldehyde-based Schiff bases.[39] This downfield shift can be attributed to the electron-withdrawing effect of the nitrile (–CN) group positioned *meta* to the imine, which reduces electron density around the imine proton, leading to deshielding. The methyl ($-CH_3$) protons appear as a singlet at δ 2.46 ppm, while aromatic protons resonate in the range of δ 6.99–7.22 ppm, displaying various splitting patterns consistent with their respective chemical environments and accounting for all protons in the molecule. In the ^{13}C NMR spectrum, the imine carbon (C═N) resonates at δ 164.8 ppm. Aromatic carbon signals are observed between δ 107.1–160.2 ppm, and the methyl carbon appears at δ 20.0 ppm. These spectral features collectively support the successful formation and structural integrity of the ligand **HL**.

The FTIR spectra of the ligand **HL** and its Co(II) complex **CoL** (SI Fig. S3 and S7) reveal characteristic vibrational bands corresponding to functional groups in the compounds. In the spectrum of **HL** (Fig. S3), prominent stretching bands were observed at 3200 cm^{-1}, 2224 cm^{-1}, and 1645 cm^{-1}, corresponding to ν(O–H), ν(C≡N), and ν(C═N) vibrations, respectively.[40] Upon complexation with Co(II), the ν(O–H) band observed at 3200 cm^{-1} in the free ligand disappeared in the spectrum of **CoL** (Fig. S7), indicating

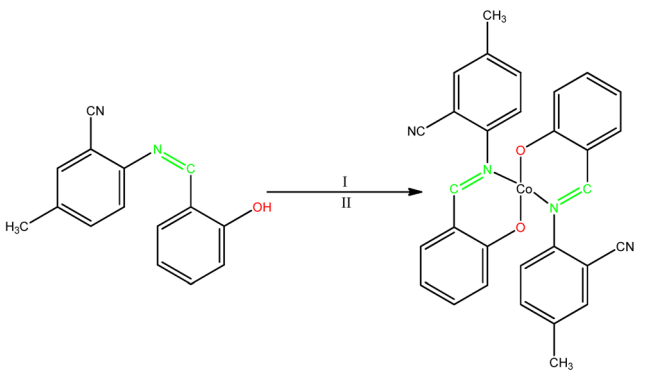

Scheme 1 Synthetic pathway showing the metallation of **HL** with Co(II) ion; I = $Co(OAc)_2{\cdot}4H_2O$, II = DCM/MeOH, 4 h, RT.

deprotonation of the hydroxyl group and its subsequent coordination with the metal ion. Additionally, the ν(C=N) stretching vibration shifted from 1645 cm^{-1} in the free ligand to 1600 cm^{-1} in the complex, reflecting a decrease in electron density on the azomethine nitrogen due to its coordination with the Co(II) centre.[41] The ν(C≡N) band also showed a slight shift, appearing at 2215 cm^{-1} in the complex, a decrease of 9 cm^{-1} compared to the free ligand. This shift can be attributed to the electronic influence of the nearby coordinated imine nitrogen, especially since the nitrile group is *meta* to the imine moiety. Moreover, two new bands appeared at 520 cm^{-1} and 463 cm^{-1} in the complex spectrum, which are assigned to ν(Co–N) and ν(Co–O) stretching vibrations, respectively.[42] These confirm the involvement of the phenolic oxygen and azomethine nitrogen atoms in coordination with the Co(II) ion, supporting the proposed structure of the complex.

The electronic absorption spectra of the compounds (SI Fig. S4 and S8) provide insight into their electronic transitions and coordination behaviour. The spectrum of the free ligand **HL** (Fig. S4) exhibits two prominent absorption bands at 215 nm and 308 nm, which are assigned to $\pi \rightarrow \pi^*$ and $n \rightarrow \pi^*$ transitions, respectively. These transitions arise from the aromatic ring and the azomethine (C=N) moiety.[42] Upon complexation with Co(II), the UV-vis spectrum of the **CoL** complex (Fig. S8) shows three absorption bands at 233 nm, 284 nm, and 524 nm. The first two bands correspond to $\pi \rightarrow \pi^*$ and $n \rightarrow \pi^*$ transitions, similar to the free ligand, but with noticeable shifts indicative of changes in the electronic environment due to coordination with the metal ion. The additional absorption band at 524 nm lies in the visible region and is attributed to a $d \rightarrow d$ transition of the Co(II) ion in the complex.[43] The redshift of the $\pi \rightarrow \pi^*$ and $n \rightarrow \pi^*$ bands, along with the emergence of the $d \rightarrow d$ transition band, provides strong evidence of ligand coordination to the Co(II) centre. These spectral changes confirm that the electronic structure of the ligand is significantly altered upon complexation, supporting successful metal–ligand interaction.

Mass spectrometric analysis was carried out to further confirm the molecular identities of the synthesized compounds. The resulting spectra are presented in SI Fig. S5 and S10. The mass spectrum of the ligand **HL** (Fig. S5) exhibits a prominent peak at m/z 237.1149, corresponding to the $[M + H]^+$ ion. This value is in excellent agreement with the calculated molecular ion peak of m/z 237.1023, thereby confirming the expected molecular weight of the ligand. Similarly, the mass spectrum of the Co(II) complex **CoL** (Fig. S10) shows a molecular ion peak at m/z 529.1086, which matches closely with the theoretical value of m/z 529.1075 for the $[M]^+$ species. The strong agreement between the experimental and calculated m/z values for both the ligand and its complex substantiates the successful synthesis and structural integrity of the compounds.

Importance of binding to HSA

Studying the binding of potential chemotherapeutics to HSA is crucial for optimizing drug pharmacokinetics, pharmacodynamics, efficacy, and toxicity. As the predominant plasma protein, HSA plays a key role in drug transport, influencing distribution, metabolism, and elimination. Bertucci *et al.*[44] demonstrated through spectroscopic and kinetic analyses that ligand binding to HSA directly influences distribution volume, metabolism, half-life, and elimination rates. HSA possesses the ability to bind a diverse range of endogenous metabolites and exogenous molecules, thereby modulating free molecule concentrations and impacting therapeutic effectiveness.[45] This dual function of HSA, acting as a reservoir for prolonged drug availability or facilitating rapid clearance, highlights the importance of assessing drug–protein interactions. A drug's strong affinity for HSA can lead to reduced free drug levels, prolonging its half-life due to reduced hepatic metabolism.[46] Thus, evaluating drug-HSA interactions is a critical first step in understanding pharmacokinetics and pharmacodynamics, offering valuable insights into therapeutic efficacy. In this study, we examined biophysical parameters governing the binding of **HL** and **CoL** to HSA using fluorescence and CD spectroscopy, contributing to the rational design of albumin-bound chemotherapeutics.

Fluorescence quenching measurements

Protein–ligand binding events can be monitored through fluorescence spectroscopy, as intrinsic protein fluorescence is sensitive to environmental perturbations. HSA contains a single tryptophan residue (Trp-214, λ^{ex} = 295 nm), located within Sudlow's site I, which serves as the principal fluorophore responsible for the protein's emission profile.[47] Fluorescence quenching can occur through static or dynamic mechanisms, or a combination thereof, depending on the nature of the interaction. In this study, the quenching behaviour of HSA (emission spectrum: 310–450 nm) was examined *via* titration with increasing concentrations of **HL** and **CoL**, revealing a distinct emission maximum at approximately 342 nm. A progressive decline in fluorescence intensity was observed as a function of ligand concentration (Fig. 1), demonstrating a dose-dependent interaction between these compounds and HSA.[48,49]

Notably, free ligand and complex binding induced a blue shift in the fluorescence emission spectrum, with both **HL** and **CoL** eliciting a spectral shift of 7 ± 1.5 nm relative to native HSA.[48] This shift suggests a transition to a less polar microenvironment around Trp-214, indicative of conformational modifications upon ligand association. Similar behaviour has been reported for HSA with other metal complexes.[48–51]

Fluorescence quenching mechanism

Fluorescence quenching is commonly described by the Stern–Volmer (SV) equation:[52]

$$I_0/I = 1 + K_{SV}[Q] = 1 + k_q\tau_0[Q] \quad (1)$$

where I_0 represents the fluorescence intensity of ligand free HSA, and I corresponds to the fluorescence intensity of HSA in the presence of **HL** and **CoL**. K_{SV} is the Stern–Volmer constant (M^{-1}), [Q] is the molar concentration of the quencher (M), k_q is the bimolecular quenching rate constant (M^{-1} s^{-1}), and τ_0 is the average lifetime of HSA fluorescence in the absence of any quencher (5.28 ± 0.03 ns,[53] 5.60 ± 0.10 ns,[54] 6.72 ± 0.07 ns,[55] mean = 5.87 ± 0.76 ns). Stern–Volmer plots recorded as a

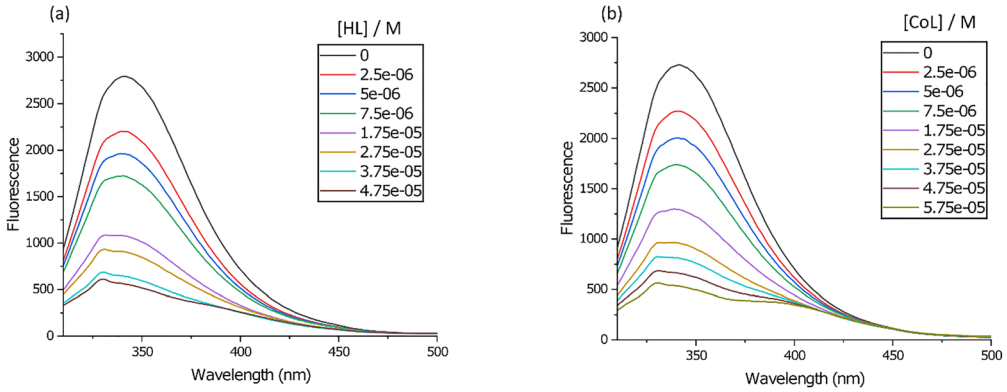

Fig. 1 (a) Emission spectra of HSA (5.0 μM) recorded as a function of the concentration of (a) **HL** and (b) **CoL** at 310 K in KH_2PO_4 (50 mM, pH 7.50).

function of temperature and ligand concentration [**HL**] and [**CoL**] are presented in Fig. 2a and b, respectively, summarising the triplicate averages of fluorescence ratio measurements at varying ligand concentrations. Typically, a linear SV plot indicates a single dominant quenching mechanism, either dynamic or static. Here, both **HL** and **CoL** exhibit linear Stern–Volmer behavior, suggesting a single dominant mechanism. Furthermore, the K_{SV} values (Table 1) increase with temperature, which is consistent with a dynamic quenching mechanism, which occurs *via* collisional interactions with the excited-state fluorophore (Trp-214). Increased thermal motion enhances molecular collisions, thereby raising quenching efficiency, as reflected in the rising K_{SV} values.

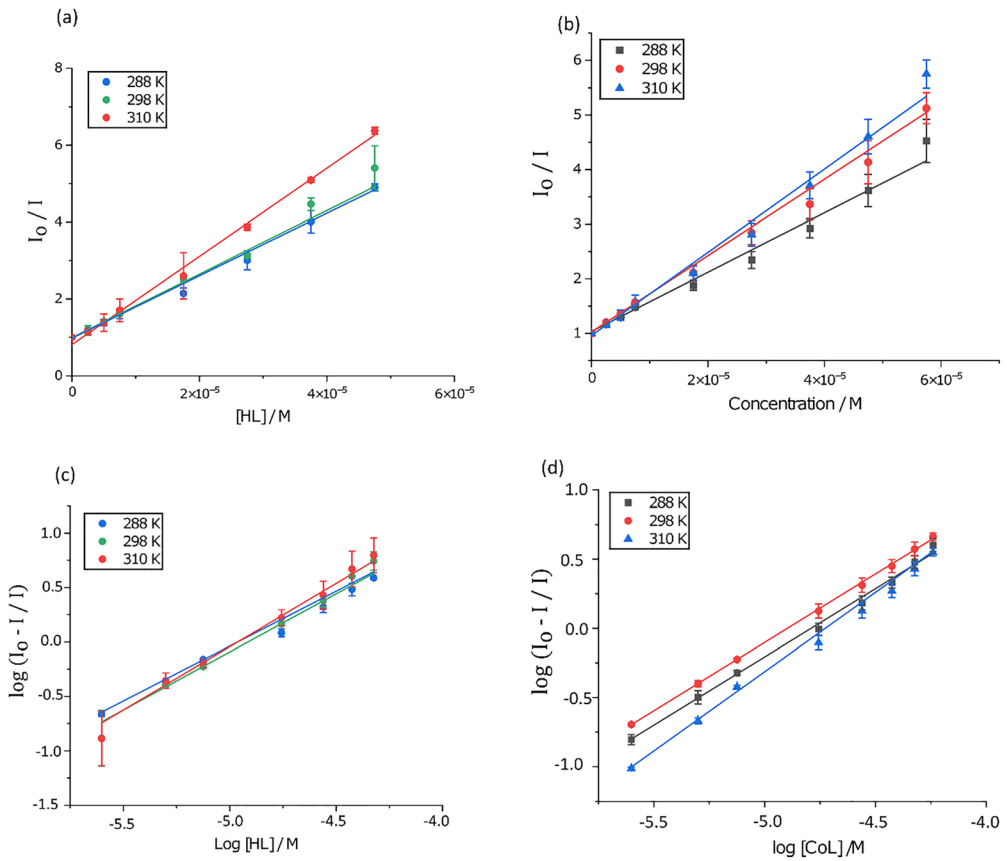

Fig. 2 Stern–Volmer (SV) fluorescence intensity ratio plots for HSA (3.0 μM) recorded as a function of the concentration of (a) **HL** and (b) **CoL** and temperature (50 mM KH_2PO_4, pH 7.50). Error bars are ESD's based on the average of three independent determinations. The data throughout the concentration range was well-fitted by eqn (1). Double logarithm plot of the fractional change in fluorescence intensity for HSA (5.0 μM) recorded as a function of the concentration of (c) **HL** and (d) **CoL** and temperature (50 mM KH_2PO_4, pH 7.50). Error bars are ESD's based on the average of three independent determinations. The data are described by eqn (3), which affords the affinity constant and stoichiometric coefficient for the reaction (Table 1).

The bimolecular fluorescence quenching rate constant (k_q) was derived from least-squares fitting of eqn (1) to dose-dependent fluorescence quenching data using the reported τ_0 value:

$$k_q = K_{SV}/\tau_0 \quad (2)$$

The k_q values for both **HL** and **CoL** exceed the diffusion-controlled limit (1×10^{10} M^{-1} s^{-1})[56] by 2 to 3 orders of magnitude, which is consistent with significant HSA–ligand binding interactions rather than non-specific diffusion-controlled collisional interactions.[57] The K_{SV} and k_q values were comparable to similar molecules previously reported.[58,59] A summary of the K_{SV} and k_q values obtained for the interaction of both compounds with HSA is reported in Table 1.

Ligand binding equilibrium constants

To further elucidate ligand-binding equilibria, fluorescence emission changes were analyzed using a double logarithmic plot approach, employing eqn (3):

$$\log\left(\frac{I_0 - I}{I}\right) = \log K_a + n\log[Q] \quad (3)$$

where the slope (n) provides the binding stoichiometry, and the intercept yields the affinity constant (K_a). The results, summarized in Table 1, indicate increasing affinity constants (K_a) with rising temperature, supporting a dynamic quenching mechanism. A point of note is that the postulated dynamic quenching mechanism is inferred solely from the temperature dependence of K_{SV} and $\log K_a$. Ideally, time-resolved fluorescence measurements of the Trp-214 fluorescence lifetime should be performed to unambiguously confirm the quenching mechanism. However, such measurements could not be conducted due to the unavailability of a time-resolved fluorometer in our laboratory. Though a mixed quenching mechanism cannot be ruled out based on the k_q value exceeding 1×10^{10} M^{-1} s^{-1}.

Notably, **HL** consistently exhibits higher $\log K_a$ values than **CoL** across all temperatures, confirming stronger binding interactions. Additionally, the binding stoichiometry were not delineated from the double log plot as it is widely reported to erroneously miscalculate the correct stoichiometry.[60] Therefore, the binding stoichiometry was delineated from the site displacement assay in Fig. 3. The comparatively lower K_{SV}, k_q, and $\log K_a$ values for **CoL** relative to **HL** suggest that cobalt coordination decreases binding affinity. Metal complexation is known to modify ligand-protein interactions through steric hindrance, electronic effects, and altered hydrophobicity. In the case of **CoL**, structural rigidity introduced by cobalt coordination may reduce ligand accessibility at the HSA binding site, leading to weaker interactions.

Table 1 Stern–Volmer quenching constants (K_{SV}), bimolecular quenching rate constants (k_q), and affinity constants ($\log K_a$) for the interaction of **HL** and **CoL** with HSA at different temperatures in 50 mM KH_2PO_4 buffer at pH 7.50

Compound	Temperature	K_{SV}[ac] ($\times 10^4$) M^{-1}	k_q[bc] ($\times 10^{13}$) M^{-1} s^{-1}	$\log K_a$[c]
	288	8.38 (0.004)	1.43	4.92 (0.16)
HL	298	9.96 (0.07)	1.70	5.01 (0.07)
	310	13.5 (0.05)	2.30	5.13 (0.001)
	288	5.87 (0.04)	1.00	4.77 (0.04)
CoL	298	6.73 (0.07)	1.15	4.83 (0.18)
	310	8.04 (0.001)	1.20	4.90 (0.07)

[a] K_{SV} values were determined by fitting the data to nonlinear eqn (2) to the data. [b] A mean excited state lifetime, τ_0, of 5.87(76) ns for HSA was used to calculate the bimolecular quenching rate constant, k_q. [c] The standard deviations are of three independent experiments.

Probe displacement assays to determine the main CoL and HL binding sites

Based on the binding constants of **CoL** and **HL** presented in Table 1, it is likely that the ligands bind to HSA in close enough proximity to quench Trp-214 fluorescence. This hypothesis was tested by performing a competitive blocking assay (site displacement assay) using fluorescence spectroscopy. For the assay, the ligands were titrated into a solution of native HSA and solutions of HSA that were pre-equilibrated with site-specific markers, warfarin and ibuprofen. Both warfarin and ibuprofen have been shown to bind to Subdomain IIA[61] and IIIA,[62] respectively, using X-ray crystallography. It should be noted that ibuprofen has a secondary binding site that it can occupy in high concentrations located between subdomains IIA and IIB.[62]

One provision is that HSA has numerous ligand-binding sites,[64] which could make interpreting the data difficult. The idea here, is that the displacement of either probes (warfarin (Fig. 3a and b)) or ibuprofen (Fig. 3d and e) by the incoming ligands would signal binding to either Sudlow's site I or II. However, if the presence of either warfarin or ibuprofen may redirect the ligand to an alternate binding site within HSA (or prevents **HL**/**CoL** uptake due to allosteric inhibition), the exact binding site may be difficult to elucidate. Although there may be certain limitations, examining alterations in the maxima wavelength peak movements of the fluoroprobe could reveal a plausible binding location for the desired ligand.

The intricate system of the ligands binding to HSA has been summarised in Fig. 3. Initially, when either **HL** or **CoL** react with native HSA, all ligand binding sites are available for complexation. According to the site displacement assay, both warfarin and ibuprofen appear to be displaced as the fluorescence of the site-specific probes for both molecules is quenched. Furthermore, we initially observe fluorescence maxima peaks for HSA{warfarin} and HSA{ibuprofen} at 388 and 335 nm, respectively. This is an 8 nm blue shift from free warfarin and a 45 nm red shift from free ibuprofen. Once either **CoL** or **HL** is titrated in, we observe the maxima peaks shifting from HSA{warfarin/ibuprofen} to the free form of the probes.

Our interpretation of this is that the incoming **CoL** or **HL** cannot be quenching the luminescent probes fluorescence by FRET, but rather displacement. Analysis of the data suggests that the ligands can target both Sudlow's sites I and II. However, since ibuprofen can occupy both sites, there is a possibility HSA's third binding site may be targeted by the ligands. While the current spectroscopic data cannot pinpoint the preferred binding site with absolute certainty, our *in silico* docking study and induced UV-CD study suggest that both sites are accessible, but warfarin (Sudlow's site I) is preferred (Fig. 6 and 7).

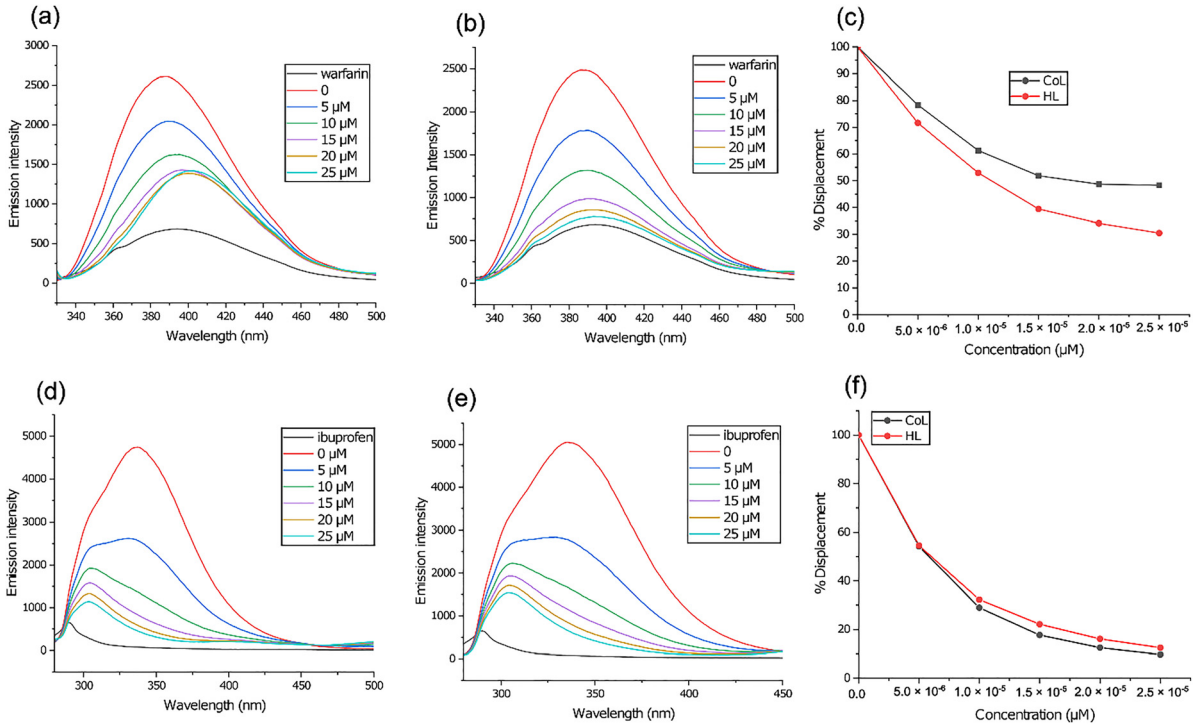

Fig. 3 Binding site determination for the reaction of **CoL** and **HL** with HSA (5.0 μM protein, 50 mM KH_2PO_4, pH 7.50, 298 K). Emission spectra of HSA···warfarin (5.0 μM warfarin λ^{ex} = 320 nm) recorded as a function of the concentration of (a) **CoL** and (b) **HL** at 310 K. (c) Both **CoL** and **HL** displace warfarin bound to HSA. Both ligands (0–25 × 10^{-6} M) were titrated into a solution containing 5 μM HSA bound to 5 μM of warfarin. Displacement of warfarin resulted in the fluorophores fluorescence being quenched. Emission spectra of HSA···ibuprofen (5.0 μM ibuprofen λ^{ex} = 263 nm) recorded as a function of the concentration of (d) **CoL** and (e) **HL** at 310 K. (f) Both **CoL** and **HL** displace ibuprofen bound to HSA. Both ligands (0–25 × 10^{-6} M) were titrated into a solution containing 5 μM HSA bound to 5 μM of ibuprofen. Displacement of ibuprofen resulted in the fluorophores fluorescence being quenched.

Lastly, the site displacement curves (Fig. 3c and f) indicate that **HL** may have a higher affinity for Sudlow's site I (warfarin binding site) as **HL** is more effective at displacing warfarin as compared to **CoL**. In the case of ibuprofen, both **CoL** and **HL** are equally as good at displacing ibuprofen.

Thermodynamics of ligand binding

The interaction between potential drug molecules and plasma proteins is governed by thermodynamic parameters that define binding affinity and molecular interactions. To elucidate the driving forces behind the binding of **HL** and its cobalt complex (**CoL**) to human serum albumin (HSA), the temperature dependence of the affinity constants (K_a) was analyzed using van't Hoff plots (Fig. 4a). A linear van't Hoff relationship was observed for both **HL** and **CoL**, indicating a single predominant binding mode. Under non-standard conditions, the enthalpy change (ΔH), entropy change (ΔS), and Gibbs free energy change (ΔG) were derived from the van't Hoff equation:

$$\ln K_a = -\frac{\Delta H}{RT} + \frac{\Delta S}{R} \quad (4)$$

where K_a is the equilibrium binding constant, R is the universal gas constant, and T represents absolute temperature. The Gibbs free energy (ΔG) was determined using:

$$\Delta G = \Delta H - T\Delta S \quad (5)$$

The Gibbs free energy values for **HL** and **CoL** are negative across all temperatures, indicating that binding to HSA is spontaneous under physiological conditions (Table 2). Notably, **HL** exhibits lower ΔG values than **CoL** at all temperatures. This suggests that **HL** binding is thermodynamically more favourable, consistent with the higher K_a values observed for **HL** relative to **CoL**.

The enthalpy (ΔH) and entropy (ΔS) components provide insight into the nature of ligand-protein interactions. The binding of **HL** to HSA is characterized by a positive enthalpy change (ΔH = 16.34 kJ mol^{-1}), coupled with a positive entropy change (ΔS = 44.7 J K^{-1} mol^{-1}). These values indicate that the biding of **HL** to HSA is entropically driven, but entropy binding must also be accounted for. The thermodynamic binding data suggests that hydrophobic interactions are the main driving force as well as conformational changes, and desolvation of ordered water molecules from HSA will also contribute to complex binding. In contrast, **CoL** displays a lower enthalpy change (ΔH = 10.36 kJ mol^{-1}) and reduced entropy contribution (ΔS = 38 J K^{-1} mol^{-1}), implying a weaker affinity *via* hydrophobic interactions, while still maintaining that it is still an entropically governed binding mechanism.

The pronounced differences in ΔH and ΔS between **HL** and **CoL** underscore the impact of cobalt complexation on ligand binding. **HL**, as a free ligand, exhibits greater conformational flexibility, allowing for increased hydrophobic interactions and entropy gains upon binding. Metal coordination in **CoL** likely

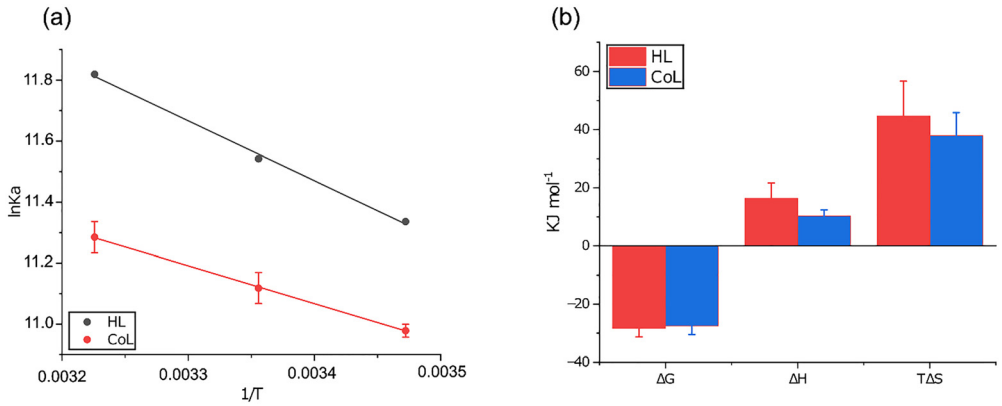

Fig. 4 (a) Linear van't Hoff plots for the reactions of **HL** and **CoL** with HSA in 50 mM KH_2PO_4 buffer at pH 7.50. (b) Comparison of the thermodynamic parameters (298 K) governing the reactions of **HL** and **CoL** with HSA. All measurements were done in triplicate, derived parameters were individually averaged, and error bars indicate standard deviations from three independent experiments.

Table 2 Thermodynamic parameters for the binding of **HL** and **CoL**, by HSA in 50 mM KH_2PO_4 buffer at pH 7.50

Compound	Temperature	ΔG^a (kJ mol^{-1})	ΔH^a (kJ mol^{-1})	$T\Delta S^a$ (J K^{-1} mol^{-1})
	288	−26.86		
HL	298	−28.36	16.34 (4.3)	0.15 (0.016)
	310	−30.16		
	288	−26.22		
CoL	298	−27.49	10.36 (2)	0.127 (0.08)
	310	−29.01		

[a] The standard deviation of three independent experiments is given in parentheses.

induces structural rigidity, reducing entropic contributions and leading to a lower overall affinity for HSA.

Far-UV CD spectroscopy

A proteins secondary structure can be elucidated using far-UV CD spectroscopy, which takes advantage of a proteins peptide bonds, aromatic amino acids side chains, and disulphide bonds.[63] HSA secondary structure is dominated by α-helices constituting 67% of its structure.[64] In Fig. 5, we employed far-UV CD spectroscopy with a spectral acquisition of 186–260 nm to delineate the impact of the free ligand (**HL**), and Co^{II} Salicaldehyde complex (**CoL**) on HSA's secondary structure.

The far-UV CD spectrum of native HSA displayed the characteristic double minima at 209 ± 1 nm and 221 ± 1 nm, consistent with a dominantly α-helix rich protein.[65] Noticeable transitions at 208 and 222 nm were assigned to π–π* and n–π* transitions, respectively. The π–π* transition at 193 nm was not observed at 1 μM HSA due to high absorbance, but this concentration was required to accurately compare the influence of **HL** and **CoL** across the 0.5–20 molar equivalent range. At a lower concentration of 300 nM HSA, the π–π* transition at 193 nm became visible.[5] Both observed transitions involve the amide groups of the peptide backbone.[63,65] To ensure the lack of the maxima at 193 nm did not interfere with the determination of the proteins secondary structure, HSA was analysed from 200–260 nm using JWMVS-529 Protein Secondary Structure Analysis program within JASCO's Spectra Manager™ package (supplied with the spectrometer). This allowed us to evaluate the changes in the secondary structure of HSA, and analyse the spectra using JASCO Spectra Manager™.[66] This allows us to

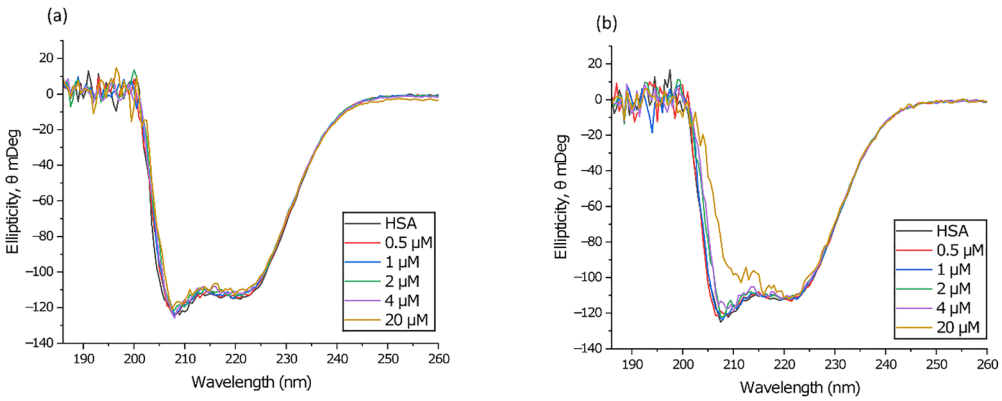

Fig. 5 Plots of the far-UV CD spectra of native HSA and the protein incubated with saturating doses of (a) **HL** and (b) **CoL** recorded at 298 K in 50 mM KH_2PO_4 buffer at pH 7.5 The concentration of both molecules ranged from 0–20 μM. To show 5% acetonitrile has a minimal effect on the structure of HSA, a control far-UV-CD is presented in the SI (Fig. S13).

Table 3 Summary of the secondary structure compositions (far UV-CD data) determined for HSA in the presence of increasing doses of **HL** and **CoL**

Compound	Concentration (μM)	α-Helix	Turn	Unordered coils
HL	0	54.61	12.27	33.12
	0.5	54.28	12.32	33.40
	1	53.83	12.45	33.72
	2	53.57	12.48	33.95
	4	53.35	12.28	34.37
	20	53.28	12.43	34.29
CoL	0	54.61	12.27	33.12
	0.5	53.44	12.32	34.24
	1	53.35	12.28	34.37
	2	53.28	12.43	34.29
	4	52.80	12.56	34.64
	20	51.46	13.10	35.44

calculate HSA's percentage composition of α-helical coils, turns, and random coils present for each HSA···ligand complex. Secondary structure domains of note were α-helices (∼54.6%), turns (12.3%) and unordered coils (∼33.1%). From Fig. 5a, and Table 3, uptake of **HL** by HSA negligibly impacts the secondary structure of the protein, reducing the α-helix content by 1.3% despite the moderately high affinity of **HL** for HSA ($\log K_a$ = 5.13; Table 1). However, in the case of **CoL**, we observe a decrease in α-helicity content as a function of **CoL** concentration (Table 3) despite **CoL** having a lower binding affinity for HSA ($\log K_a$ = 4.90; Table 1). In both cases, the decrease in α-helicity was accompanied by an increase in turns and unordered coils. Interestingly, the solution-state secondary structure composition of HSA differs from that of native HSA in the solid state[67] (68.5% α-helix, 0% β-sheet, 9.6% turns, and 21.9% unordered coils; PDB code 1BM0, analysed with BeStSel[68]). However, our solution phase far-UV CD data are consistent with solution state spectral decompositions reported previously.[69–71] Overall, it is accepted that enhanced subdomain mobility and general thermal motion/disorder accounts for the decrease of α-helicity seen in the solid state.[65,72]

Near UV-CD spectroscopy

To elucidate the conformational changes induced by both ligands to the tertiary structure of HSA, we employed near-UV CD spectroscopy in the range of 250–310 nm (Fig. 6a and b). A near-UV-CD spectrum is dominated by fine structure transitions from Trp (285–300 nm), Tyr (275–285 nm), Phe (250–270 nm), and Cys–Cys which tend to reflect the local symmetry of the chromophore. Significant transition peaks for HSA were observed, including two minima at 262 and 280 nm and a maximum at 290 nm, which are attributed to the presence of disulfide bonds and the aromatic amino acids.[73]

The near-UV CD spectra of HSA (Fig. 6a and b) in the absence of ligands displayed a broad peak centred at 290 nm, accompanied by distinct fine structure features between 290–305 nm, which are attributed to the Trp-214 residue. In the 275–285 nm region, a peak at 284 nm with a shoulder at 287 nm was observed, likely arising from the 18 Tyr residues present in HSA. The phenylalanine fingerprint region (255–270 nm) exhibited a peak near 257 nm. Notably, the spectrum also featured two minima at 262 and 266 nm, along with a shoulder at 279 nm, hallmarks of disulfide bonds.[63,74,75] Phe, Tyr, and Trp residues are characterized by π–π* electronic transitions (^1L_a and ^1L_b) and are capable of participating in π-bonding, which plays a key role in ligand-protein interactions, as previously discussed. Consequently, perturbations in the fine spectral features of the protein may reflect conformational changes or modifications in the local environment of these aromatic residues.[76]

Both ligands, **HL** and **CoL**, induced changes in the near-UV CD spectra, specifically in the fine structure associated with aromatic amino acids, indicating that they bind to the protein in close enough proximity to influence the local environment of these residues. **HL** did not cause significant alterations in the disulfide bond fingerprint region, suggesting minimal disruption to these bonds. Glide XP docking of **HL** to HSA (Fig. 6c) closely corroborated the near-UV CD spectral data of **HL** binding (Fig. 6a). As shown in Fig. 6c, **HL** is positioned within 8 Å of Trp-214, five Tyr residues, and two Phe residues, accounting for the observed perturbations in HSA's fine structure at approximately 260, 280, and 295 nm, respectively. Furthermore, no Cys–Cys disulfide bonds were found within 8 Å of **HL**.

Similarly, docking analysis of **CoL** with HSA revealed that Trp-214, three Tyr residues, and three Phe residues are located within 8 Å of the binding site. Notably, the perturbation observed in the disulfide bond fine structure around 266 nm can be attributed to the presence of three disulfide bonds in close proximity to **CoL** within the protein structure (Fig. 6d). Overall, the binding of both ligands to HSA was shown to induce slight conformational changes in both the secondary (Fig. 5) and tertiary structures (Fig. 6) of the protein. These conformational changes in the tertiary structure may account for the displacement of ordered water molecules and a change in the proteins flexibility, therefore responsible for the driving of force of the molecules being hydrophobic interactions and the differences observed in our thermodynamic data.[77]

An interesting observation from Fig. 6c and d indicates that some of the residues interacting with both **CoL** and **HL** are found in ibuprofen secondary binding site (Phe211, Arg218, Leu219, Tyr150, His242, Lys195)[62] as well as residues in Sudlow's site I. The near UV-CD data suggest that both ligands likely target Sudlow's site I and Sudlow's site II or potentially HSA's secondary ligand binding site.

Molecular docking and molecular dynamic simulations

Theoretical ligand docking studies were employed using Glide XP to determine the binding mode of **HL** and **CoL** to HSA. The X-ray structure was used (PDB: 1HA2 (2.50 Å)) for flexible ligand docking. It should be noted that ligand docking provides only an approximation as to how a ligand may bind to and interact with a specific protein. The major parameter elucidated from ligand docking is the docking scores, which typically do not correlate quantitatively with experimental binding or thermodynamic data (K_a or ΔG values).[78,79] This is because ligand docking does not try to emulate a physical reaction between the incoming ligand and macromolecule. Hence, only qualitative

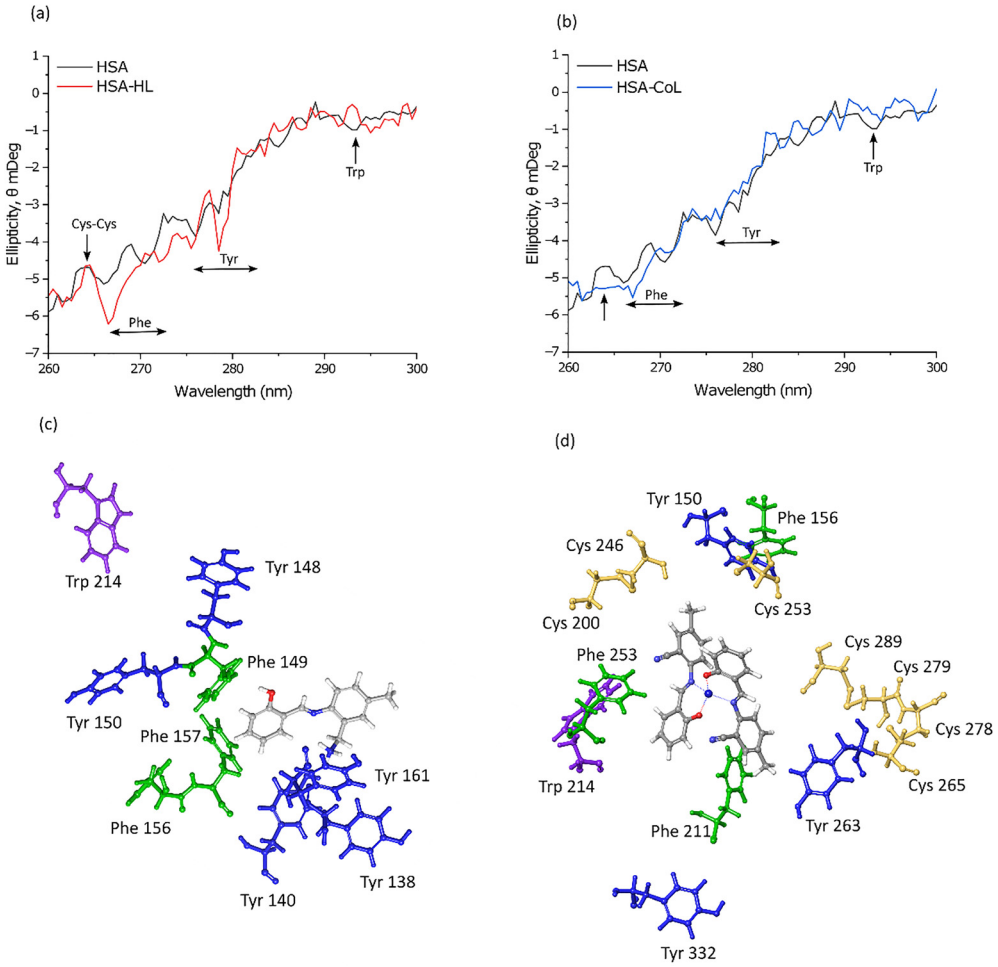

Fig. 6 Plots of the near-UV CD spectra of native HSA and the protein incubated with a 1 : 1 ratio of (a) **HL** and (b) **CoL** were recorded at 298 K in 50 mM KH_2PO_4 buffer at pH 7.50. The data represents unsmoothed spectra in the fine structure region for the protein. Perturbations in the protein structure around Phe (250–270 nm), Tyr (~280 nm), and Trp (285–300 nm) residues are evident. GLIDE XP docking analysis of the binding of (c) **HL** and (d) **CoL** to HSA using the X-ray structure of HSA as the *in silico* target (PDB code 1HA2). A large target grid was generated for macromolecular ligand docking at the warfarin site (with warfarin removed), spanning 40 × 40 × 40 $Å^3$. The image panels show selected aromatic acid residues and cysteine residues within 8 Å as the binding of both ligands will perturb these residues transitions.

comparisons can be made from docking scores. In our case, we aim to determine if the Glide XP docking scores corroborate our experimental data and shows **HL** and **CoL** interacting with HSA.

The key results are that **CoL** and **HL** binds to HSA in Sudlow's site I and II, or ibuprofen secondary binding site domain IB, just outside Sudlow's site I, but still in close enough proximity of Trp-214 to quench its intrinsic fluorescence by FRET. The *in silico* work corroborated the fluorescence quenching data (*vide supra*). However, to ensure this data was significant we opted to use a MD simulation. Following ligand docking, a 100 ns molecular dynamics (MD) simulation (Fig. 7 and 8) was conducted to assess the stability of the best Glide XP docking pose (Fig. 7). MD simulations provide valuable insights into the interactions between macromolecules and ligands over time, capturing the system's dynamic behaviour and offering a more accurate reflection of physiological conditions. Following the 100 ns trajectory the best pose is presented in Fig. 7.

Following this, the trajectory frames of the HSA:**HL** and HSA:**CoL** systems were analyzed for protein RMSD by calculating the average distance of the Cα atoms in each frame relative to a reference frame. The analysis was performed using a 100 ns molecular dynamics simulation under isothermal–isobaric (NPT) conditions at ~1 bar and 300 K, employing the OPLS_2005 force field and the TIP3P solvent model. The protein RMSD values for both systems were plotted over the 100 ns simulation period (Fig. 8a and b). The trajectories showed fluctuations of less than 1.5 Å after reaching a plateau, indicating that the systems were well-equilibrated. These low RMSD values also confirm the structural stability of both HSA:**HL** and HSA:**CoL** complexes throughout the simulation, suggesting that both ligands maintained relatively stable conformations when bound to HSA. To further understand the mechanisms of protein–ligand recognition, binding, and specificity, protein–ligand interactions were monitored and are shown in Fig. 8c and d. The interaction profiles over the 100 ns simulations reveal that both ligands were

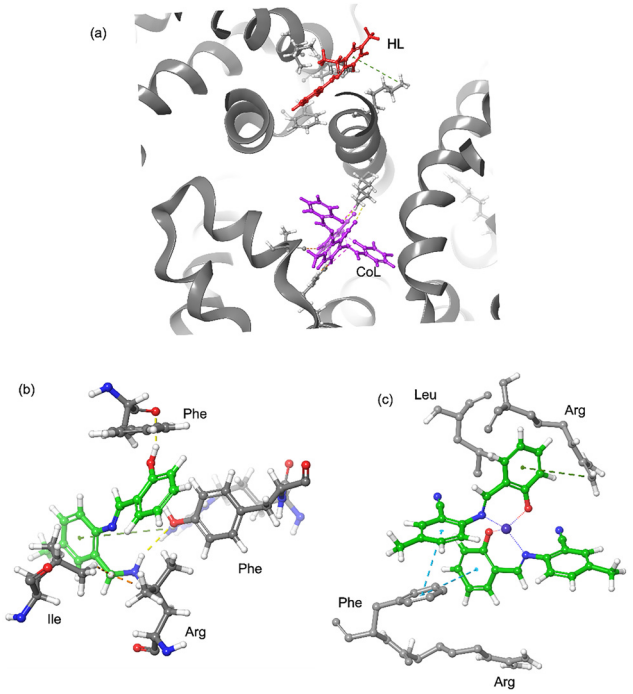

Fig. 7 (a) Most stable docked pose of **HL** and **CoL** following molecular dynamic simulations (MD) over 100 ns of the best docked GLIDE XP structure of both ligands binding to HSA (PDB 1HA2) bound to warfarin.[80] A large target grid was generated for ligand docking at the Trp-214 residue, spanning 40 × 40 × 40 Å^3, thereby facilitating a search of alternative binding pockets radiating throughout the protein. The simulation was carried out at 310 K and pH 7.4. (b) Free ligand **HL** and (**c**) metal complex **CoL** bound to HSA, showing the amino acid residues the ligands interact with.

primarily stabilized within Sudlow's site I through a combination of interactions, predominantly hydrophobic in nature. Strikingly, the best docked pose of both ligands complements the amino acid residues both ligands are in contact with very well (Fig. 6). Even though the amino acid residues **HL** interacts with are non-polar, the main bonds present are H-bonds with the chelating oxygen and nitrogen atoms. In the case of **CoL**, we see that the aromatic ring structure π–π stacks with the phenylalanine ring structure and mainly interacts with all residues by hydrophobic interactions.

RMSF plots for the HSA:**HL** and HSA:**CoL** systems were generated by mapping side-chain fluctuations against residue numbers, using data from the 100 ns simulation trajectories. These plots serve to quantify the average movement of individual atoms, providing insights into the flexibility and dynamic behaviour of residues within each system. In both Fig. 8e and f, the overall low RMSF values suggest that the amino acid residues exhibit minimal deviation from their mean positions, indicating a high degree of structural stability. This stability implies that the regions where **HL** and **CoL** bind are well-structured and that both ligands maintain consistent conformations throughout the simulation.

Discussion relating Δ*G* directly to experimental free energies

Our thermodynamic interaction studies indicated that **HL** binds slightly more strongly to HSA than **CoL** ($\Delta G = -7.2$ kcal mol^{-1} *vs.* -6.9 kcal mol^{-1}; a difference of $\Delta G = 0.3$ kcal mol^{-1}). This small difference indicates that both ligands bind with comparable affinities. Docking results are consistent with this experimental trend: **HL** yielded a more favourable $\Delta G_{\text{docking}}$ score (-4.842) than the **CoL** (-4.048), again suggesting marginally stronger binding of the uncomplexed ligand (Table S1). Although the magnitude of docking scores cannot be compared directly to experimental ΔG values, the qualitative agreement reinforces the reliability of the observed preference.

It is important to acknowledge that docking scores are empirical scoring functions and do not represent true thermodynamic parameters of free energies. They approximate mainly enthalpic interactions and often neglect explicit solvation, entropic contributions (which is the dominant governing parameter in our current system), protein conformational flexibility, and metal-specific coordination effects. These simplifications are particularly relevant for metal complexes, where partial charges, coordination geometry, and ligand field effects are challenging to capture accurately in standard docking protocols. Experimental ΔG values, in contrast, for **HL** and **CoL** reflect entropic contributions in our phosphate buffer system and inherently include solvent reorganization and protein adaptability. Thus, the absolute difference between docking scores and experimental binding energies is expected, and the two should be compared only qualitatively.

Despite these limitations, the computational results reproduce the experimentally observed direction of binding affinity differences, supporting the conclusion that Co coordination slightly reduces the organic ligand binding to HSA. The close agreement in trend, though not magnitude, suggests that the docked binding modes are reasonable and provides a solid foundation to analyse further by MD simulations (*vide infra*). MD simulations will provide a deeper insight into the contributions of ordered waters, HSA flexibility, and metal coordination to HSA binding.

Discussion on the importance of MD studies

$\Delta G_{\text{docking}}$ scores provide a useful first indication of relative binding preferences, but they are not quantitatively reliable because they rely on simplified scoring functions, limited treatment of solvation and entropy, and often assume a rigid protein structure. As a result, $\Delta G_{\text{docking}}$ scores should be interpreted qualitatively rather than as true free energies of binding. MD compensates for these limitations by simulating the ligand–protein complex in a fully flexible, explicitly solvated environment that captures induced-fit effects, aqueous buffer interactions, and realistic metal coordination. When combined with end-point free energy methods such as MM-PBSA/MM-GBSA, MD provides thermodynamically grounded binding energy estimates that can be directly compared to experimental values, thereby overcoming the quantitative shortcomings of docking.

Discussion surrounding binding equilibrium

It is of utmost importance to study the interactions of investigational drugs with HSA, this is because about 68–98% of cisplatin binds to HSA within 24 hours of administration, according to literature studies.[81,82] This has resulted in an

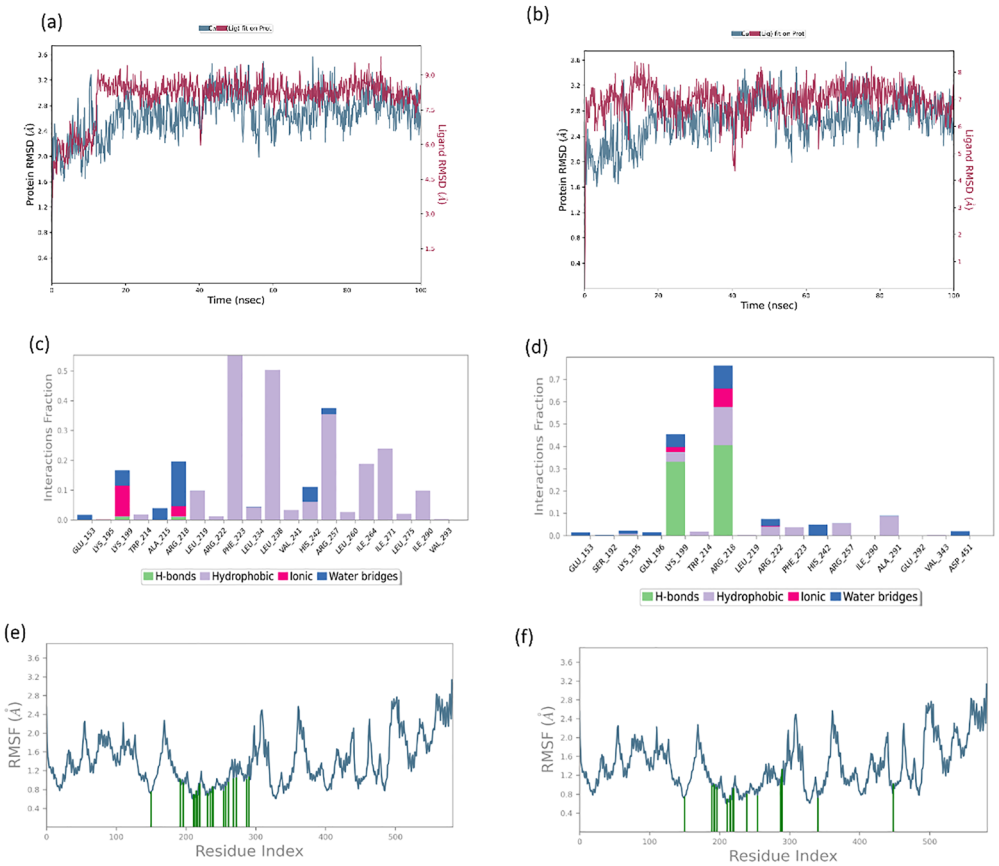

Fig. 8 Analysis of the simulation trajectory showing (a) the protein-RMSD (blue), **HL**-RMSD (red) and (b) protein-RMSD (blue), **CoL**-RMSD (green) over 100 ns. Amino acid side chains interactions and types of interactions stacked bar charts between (c) HSA:**HL** and (d) HSA:**CoL**, throughout the 100 ns simulation. The interaction diagram showed that H-bonds are categorized into backbone acceptor, backbone donor, side-chain acceptor, and side-chain donor. Hydrophobic interactions are categorized into π–cation, π–π*, and other non-specific interactions. The stacked bar charts are normalized throughout the 100 ns trajectory. The images were obtained using the ligand interaction algorithm implemented in Maestro v13.6. The protein-RMSF of the side chains as a function of the 100 ns simulation time for (e) HSA:**HL** complex (red), and (f) HSA:**CoL** complex (green). The simulation was carried out at 310 K and pH 7.4.

ongoing debate as to whether HSA acts as a reservoir for storing therapeutic agents or if it binds them, thus preventing the drug from effectively distributing to tissues and rendering the bound drug to have lower efficacy. This question has been difficult to answer as there is evidence for both arguments. Holding *et al.*[83] showed that an HSA-cisplatin adduct was still cytotoxic to carcinoma cells. However, studies by Møller *et al.*[84] showed that the HSA-cisplatin adduct was not taken up by Ehrlich Ascites Tumour Cells (EATC) and adherent Ehrlich Lettré Ascites Cells (Lettré) and did not cause cytotoxicity. Similar results were found with NHIK 3025 cells.[85]

The thermodynamic data obtained in this study provides important insight into how differential binding to serum albumin may influence the pharmacological behaviour of **HL** and its cobalt complex, **CoL**. Our results show that **HL** exhibits approximately one log unit stronger binding affinity to HSA compared to **CoL**. In a pharmacological context, stronger albumin binding generally reduces the fraction of freely available drug in circulation, as only the unbound fraction is able to diffuse into cells, engage intracellular targets, and exert cytotoxic activity.[86,87] Thus, although albumin binding can prolong circulation time, it also decreases the immediate bioavailable pool of the compound.

This concept is in agreement with our previous *in vitro* findings, where **HL** displayed markedly lower cytotoxicity and a higher IC_{50} value relative to **CoL** in MCF-7 cells (around 10-fold).[88] Cell culture media contain bovine serum albumin (BSA), which has about 76% similarity to HSA and can mirror the binding behaviour of HSA. The stronger albumin affinity of **HL** suggests that a significant portion of the ligand may be sequestered by BSA in the media, leaving a smaller free fraction capable of entering cells. As a result, the effective intracellular concentration of **HL** would be reduced despite identical nominal dosing, leading to the reduced cytotoxic response observed experimentally.

In contrast, the comparatively weaker albumin binding of **CoL** implies that a larger proportion of the drug remains unbound and bioavailable under similar conditions. This increased free fraction likely contributes to the markedly higher cytotoxic activity of **CoL** (more than 10-fold stronger than **HL** in our previous study[88]). From a pharmacological perspective, lower albumin affinity can enhance drug exposure at the cellular level,

accelerating uptake and contributing to a more potent biological response.

These findings underscore an important structural and mechanistic distinction between **HL** and **CoL**: while **HL** binds more strongly to serum proteins and is retained, **CoL** remains more freely available to interact with its biological target. This highlights the possibility that metal coordination plays a beneficial role by modulating plasma protein binding and improving bioavailability. Understanding this relationship is crucial for the rational design of future analogues, as tuning albumin-binding affinity may provide a means to optimize pharmacokinetic properties and therapeutic efficacy.

Discussion on future work with ligand design

The differential albumin binding profiles observed for **HL** and **CoL** also provide valuable design principles for future 2-(hydroxybenzylidene)amino-5-methylbenzonitrile ligands. Our current findings imply that rational tuning of the coordination sphere such as altering ligand substituents, electronic properties, or overall complex charge could offer a strategy to fine-balance albumin binding and optimize free drug levels. Since **HL** binds to HSA through both hydrogen bonding and π–π bonding, it is important to consider these functional groups' influence on the ligand-protein binding in future work. Incorporating structural elements that limit high affinity albumin binding, without compromising stability or target engagement, may therefore enhance the cytotoxic efficacy of both **HL** and **CoL** analogues.

How the potential binding of CoL may affect competition with common drugs like warfarin

The potential occupancy of Sudlow's site I or Sudlow's site II by **HL** or **CoL** has important clinical implications. Sudlow's sites I and II are primary high-affinity binding sites for several well-known pharmaceutical drugs, whose interaction with HSA has been structurally and thermodynamically characterized.[89] For example, we know both **HL** and **CoL** will bind to Sudlow's site I, which is occupied by warfarin. Occupancy of this site by another ligand could lead to competitive displacement, increasing the free (unbound) concentration of warfarin and thereby enhancing its anticoagulant effect, which may increase the risk of bleeding. This mechanism has been implicated in clinically significant interactions when highly bound drugs displace warfarin from albumin.[90] Conversely, if warfarin displaces our **CoL** complex, its pharmacokinetics could be altered, reducing bioavailability and therapeutic efficacy. From a drug-design perspective, these findings suggest that future cobalt-based analogues should be optimized not only for binding strength but also for site specificity, minimizing overlap with warfarin's binding footprint to mitigate potential drug–drug interactions. The demonstrated flexibility of the Sudlow I site to adapt to structurally diverse ligands further support the feasibility of such optimisation.

Conclusion

The interaction of **HL** and **CoL** with HSA was investigated using complementary spectroscopic techniques to understand how the Co^{II} metal influences ligand uptake by the protein as opposed to the free ligand. Both **HL** and **CoL** quenched the intrinsic Trp-214 fluorescence of HSA, *via* a dynamic quenching mechanism. **CoL** had a binding affinity constant $7.94 \times 10^4\ M^{-1}$ to HSA that was typical of many small molecule ligands for the protein (10^3–$10^5\ M^{-1}$), while **HL** had a 1.7 factor higher binding affinity of $1.35 \times 10^5\ M^{-1}$.[91,92] The Stern–Volmer quenching constants (K_{SV}) followed the order **HL** > **CoL**. The reaction stoichiometry for both ligands was 1 : 1 (**HL**/**CoL** : HSA), with possible partial occupation of a second, lower affinity site occurring at higher concentrations.

Both **HL** and **CoL** bound to HSA with a positive ΔH, negative ΔG and a positive ΔS, consistent with entropically driven binding with HSA. Glide XP docking, molecular dynamic simulations in conjunction with fluorescence and UV-CD showed that **HL** and **CoL** bind preferentially in Sudlow's site I, with possible additional binding sites being accessible. Far- and near-UV CD spectroscopy confirmed that the binding of **HL** and **CoL** minimally perturbs the protein's secondary structure.

These complementary experimental and *in silico* findings provide mechanistic insight into how metal coordination modulates protein–ligand interactions. From a drug development perspective, this knowledge can guide the rational design of cobalt-based therapeutics by tuning albumin binding affinity to optimize pharmacokinetics, therapeutic efficacy, and safety, while minimizing potential drug–drug interactions at high-affinity binding sites such as Sudlow's site I. Overall, the combined biophysical and *in silico* framework presented here offers a predictive strategy for designing metallodrugs with improved *in vivo* performance.

Finally, the biophysical data distinctly confirm uptake of the intact complexes without hydrolysis or demetallation and the binding affinity of **HL** to HSA may result in the ligands lower bioavailability *in vitro*. The higher HSA binding affinity of **HL** has important pharmacokinetic implications: suggesting that a larger fraction of **HL** may remain bound to albumin in plasma, reducing its free-drug concentration, slowing tissue distribution, and potentially delaying cellular uptake, which could contribute to its higher IC_{50} *in vitro*. In contrast, **CoL** exhibits weaker binding, suggesting a greater free-drug fraction that may enhance tissue penetration, cytotoxic activity, and therapeutic efficacy. These findings highlight that metal coordination can modulate ligand–protein interactions, and that tuning albumin binding may be a useful strategy to optimize the pharmacokinetic and therapeutic profiles of cobalt-based drugs.

Author contributions

S. S., I. W., A. J. M. and M. N. conceived the study I. W. synthesised and characterised the compounds. S. S. performed HSA spectroscopy, thermodynamics measurements, *in silico* studies and analyzed all biophysical data. S. S. and I. W. drew figures. S. S., I. W., M. N. wrote the paper in parts. The final editing by S. S., A. J. M. and M. N. Finally, A. J. M. and M. N. directed and secured funding for the research programme.

Conflicts of interest

There are no conflicts to declare.

Data availability

Data will be available on request.

The data supporting this article have been included as part of the supplementary information (SI). Supplementary information: complete experimental details. See DOI: https://doi.org/10.1039/d5nj03624k.

Acknowledgements

The authors thank WITS University and the NRF for funding to purchase a JASCO J-1500 MCD spectrometer (Grant No. 116177, OQM). We also thank the Centre for High Performance Computing (Project CHEM1633, CHPC, Cape Town) for both the CPU time and resources needed for the DFT simulations.

References

1 S. Dilruba and G. V. Kalayda, Platinum-Based Drugs: Past, Present and Future, *Cancer Chemother. Pharmacol.*, 2016, **77**, 1103–1124.
2 S. Ambika, Y. Manojkumar, S. Arunachalam, B. Gowdhami, K. K. Meenakshi Sundaram, R. V. Solomon, P. Venuvanalingam, M. A. Akbarsha and M. Sundararaman, Biomolecular Interaction, Anti-Cancer and Anti-Angiogenic Properties of Cobalt(III) Schiff Base Complexes, *Sci. Rep.*, 2019, **9**, 2721.
3 A. Casini and A. Pöthig, Metals in Cancer Research: Beyond Platinum Metallodrugs, *ACS Cent. Sci.*, 2024, **10**, 242–250.
4 K. Kar, D. Ghosh, B. Kabi and A. Chandra, A Concise Review on Cobalt Schiff Base Complexes as Anticancer Agents, *Polyhedron*, 2022, **222**, 115890.
5 S. Sookai, M. Akerman, M. Færch, Y. Sayed and O. Q. Munro, Cytotoxic Pyrrole-Based Gold(III) Chelates Target Human Topoisomerase II as Dual-Mode Inhibitors and Interact with Human Serum Albumin, *Eur. J. Med. Chem.*, 2025, 117330.
6 S. Sookai, M. P. Akerman, Q. Munro and O. Chiral, Au(III) Chelates Exhibit Unique NCI-60 Cytotoxicity Profiles and Interactions with Human Serum Albumin, *Dalton Trans.*, 2024, **53**, 5089–5104, DOI: 10.1039/D3DT04024K.
7 S. Wongsuwan, J. Chatwichien, W. Sirisaksoontorn, K. Chainok, A. Songsasen and R. Chotima, Novel Pd(II) Pincer Complexes Bearing Salicylaldimine-Based Benzothiazole Derivatives: Synthesis, Structural Characterization, DNA/BSA Binding, and Biological Evaluation, *New J. Chem.*, 2023, **47**, 10624–10637.
8 L. Zeng, P. Gupta, Y. Chen, E. Wang, L. Ji, H. Chao and Z.-S. Chen, The Development of Anticancer Ruthenium(II) Complexes: From Single Molecule Compounds to Nanomaterials, *Chem. Soc. Rev.*, 2017, **46**, 5771–5804.
9 F.-X. Wang, M.-H. Chen, X.-Y. Hu, R.-R. Ye, C.-P. Tan, L.-N. Ji and Z.-W. Mao, Ester-Modified Cyclometalated Iridium(III) Complexes as Mitochondria-Targeting Anticancer Agents, *Sci. Rep.*, 2016, **6**, 38954.
10 C. Marzano, M. Pellei, F. Tisato and C. Santini, Copper Complexes as Anticancer Agents, *Anti-Cancer Agents Med. Chem.*, 2009, **9**, 185–211, DOI: 10.2174/187152009787313837.
11 P. Ji, P. Wang, H. Chen, Y. Xu, J. Ge, Z. Tian and Z. Yan, Potential of Copper and Copper Compounds for Anticancer Applications, *Pharmaceuticals*, 2023, **16**, 234.
12 M. Ulular, N. Sarı, F. Han, H. Öğütçü and E. Hasanoğlu Özkan, Synthesis, Antimicrobial, and DNA-Binding Evaluation of Novel Schiff Bases Containing Tetrazole Moiety and Their Ni(II) and Pt(II) Complexes, *Pharm. Chem. J.*, 2024, **57**, 1609–1620.
13 Y.-T. Chen, S.-N. Zhang, Z.-F. Wang, Q.-M. Wei and S.-H. Zhang, Discovery of Thirteen Cobalt(II) and Copper(II) Salicylaldehyde Schiff Base Complexes That Induce Apoptosis and Autophagy in Human Lung Adenocarcinoma A549/DDP Cells and That Can Overcome Cisplatin Resistance in Vitro and in Vivo, *Dalton Trans.*, 2022, **51**, 4068–4078.
14 D. Śmiłowicz and N. Metzler-Nolte, Bioconjugates of Co(III) Complexes with Schiff Base Ligands and Cell Penetrating Peptides: Solid Phase Synthesis, Characterization and Antiproliferative Activity, *J. Inorg. Biochem.*, 2020, **206**, 111041, DOI: 10.1016/j.jinorgbio.2020.111041.
15 Marmion, C. J. A. Sigel, H. Sigel and R. K. O. Sigel, Interrelations between Essential Metal Ions and Human Diseases. Vol. 13 of Metal Ions in Life Sciences: Springer, Dordrecht, 2013, 573 Pp,[ISSN: 1559-0836, ISSN (Electronic) 1868-0402],[ISBN 978-94-007-7499-5, ISBN (e-Book) 978-94-007-7500-8, DOI , DOI: 10.1007/978-94-007-7500-8]2014.
16 C. R. Munteanu and K. Suntharalingam, Advances in Cobalt Complexes as Anticancer Agents, *Dalton Trans.*, 2015, **44**, 13796–13808.
17 H. Glasner and E. Y. Tshuva, A Marked Synergistic Effect in Antitumor Activity of Salan Titanium(IV) Complexes Bearing Two Differently Substituted Aromatic Rings, *J. Am. Chem. Soc.*, 2011, **133**, 16812–16814.
18 H. Glasner and E. Y. Tshuva, C 1-Symmetrical Titanium(IV) Complexes of Salan Ligands with Differently Substituted Aromatic Rings: Enhanced Cytotoxic Activity, *Inorg. Chem.*, 2014, **53**, 3170–3176.
19 A. P. King, H. A. Gellineau, J.-E. Ahn, S. N. MacMillan and J. J. Wilson, Bis (Thiosemicarbazone) Complexes of Cobalt(III). Synthesis, Characterization, and Anticancer Potential, *Inorg. Chem.*, 2017, **56**, 6609–6623.
20 M. D. Hall, T. W. Failes, N. Yamamoto and T. W. Hambley, Bioreductive Activation and Drug Chaperoning in Cobalt Pharmaceuticals, *Dalton Trans.*, 2007, 3983–3990.
21 B. Sahu, R. Sahu, B. Gidwani and A. Mishra, Pyrrole: An Essential Framework in the Development of Therapeutic Agents and Insightful Analysis of Structure-Active Relationships, *ChemistrySelect*, 2024, **9**, e202401604.
22 N. Jeelan Basha, S. M. Basavarajaiah and K. Shyamsunder, Therapeutic Potential of Pyrrole and Pyrrolidine Analogs: An Update, *Mol. Diversity*, 2022, **26**, 2915–2937.
23 S. Y. Lawan, M. B. Mshelia, G. A. Mala, W. O. Olaide, S. A. Musa, A. A. Ahmed, H. B. Yesufu and I. Waziri, Antioxidant Activity and DFT Calculations of Metal Complexes Derived

from a Schiff Base Ligand: Synthesis, Characterization, and Biological Evaluation, *ChemistrySelect*, 2024, **9**, e202400676, DOI: 10.1002/slct.202400676.

24 T. A. Martin and W. G. Jiang, Hepatocyte Growth Factor and Its Receptor Signalling Complex as Targets in Cancer Therapy, *Anti-Cancer Agents Med. Chem.*, 2010, **10**, 2–6.

25 A. Catalano, M. S. Sinicropi, D. Iacopetta, J. Ceramella, A. Mariconda, C. Rosano, E. Scali, C. Saturnino and P. Longo, A Review on the Advancements in the Field of Metal Complexes with Schiff Bases as Antiproliferative Agents, *Appl. Sci.*, 2021, **11**, 6027.

26 M. Yadav, D. Yadav, D. P. Singh and J. K. Kapoor, Pharmaceutical Properties of Macrocyclic Schiff Base Transition Metal Complexes: Urgent Need in Today's World, *Inorg. Chim. Acta*, 2023, **546**, 121300.

27 J. M. Mir, S. A. Majid and A. H. Shalla, Enhancement of Schiff Base Biological Efficacy by Metal Coordination and Introduction of Metallic Compounds as Anticovid Candidates: A Simple Overview, *Rev. Inorg. Chem.*, 2021, **41**, 199–211, DOI: 10.1515/revic-2020-0020.

28 P. Durairaj, T. Maruthavanan, S. Manjunathan, S. Subashini, S. L. Rokhum and G. Baskar, Microwave Assisted Synthesis, Characterization and Bioactivity Evaluation of a Cobalt(II) Complex with a Novel Schiff Base Ligand Derived from Phenylacetyl Urea and Salicylaldehyde, *J. Mol. Struct.*, 2024, **1295**, 136650, DOI: 10.1016/j.molstruc.2023.136650.

29 T. L. Yusuf, I. Waziri, K. A. Olofinsan, E. O. Akintemi, E. C. Hosten and A. J. Muller, Evaluating the in Vitro Antidiabetic, Antibacterial and Antioxidant Properties of Copper(II) Schiff Base Complexes: An Experimental and Computational Studies, *J. Mol. Liq.*, 2023, **389**, 122845.

30 S. Curry, Lessons from the Crystallographic Analysis of Small Molecule Binding to Human Serum Albumin, *Drug Metab. Pharmacokinet.*, 2009, **24**, 342–357.

31 A. Merlino, Metallodrug Binding to Serum Albumin: Lessons from Biophysical and Structural Studies, *Coord. Chem. Rev.*, 2023, **480**, 215026.

32 G. De Simone, A. di Masi and P. Ascenzi, Serum Albumin: A Multifaced Enzyme, *Int. J. Mol. Sci.*, 2021, **22**, 10086.

33 M. R. Green, G. M. Manikhas, S. Orlov, B. Afanasyev, A. M. Makhson, P. Bhar and M. J. Hawkins, Abraxane®, a Novel Cremophor®-Free, Albumin-Bound Particle Form of Paclitaxel for the Treatment of Advanced Non-Small-Cell Lung Cancer, *Ann. Oncol.*, 2006, **17**, 1263–1268.

34 H. Cho, S. I. Jeon, C.-H. Ahn, M. K. Shim and K. Kim, Emerging Albumin-Binding Anticancer Drugs for Tumor-Targeted Drug Delivery: Current Understandings and Clinical Translation, *Pharmaceutics*, 2022, **14**, 728.

35 A. H. Bakheit, Q. Saquib, S. Ahmed, S. M. Ansari, A. M. Al-Salem and A. A. Al-Khedhairy, Covalent Inhibitors from Saudi Medicinal Plants Target RNA-Dependent RNA Polymerase (RdRp) of SARS-CoV-2, *Viruses*, 2023, **15**, 2175, DOI: 10.3390/v15112175.

36 A. H. Bakheit and H. M. Alkahtani, Integrated Structural, Functional, and ADMET Analysis of 2-Methoxy-4, 6-Diphenylnicotinonitrile: The Convergence of X-Ray Diffraction, Molecular Docking, Dynamic Simulations, and Advanced Computational Insights, *Molecules*, 2023, **28**, 6859.

37 H. S. Khalaf, A. M. Naglah, M. A. Al-Omar, G. O. Moustafa, H. M. Awad and A. H. Bakheit, Synthesis, Docking, Computational Studies, and Antimicrobial Evaluations of New Dipeptide Derivatives Based on Nicotinoylglycylglycine Hydrazide, *Molecules*, 2020, **25**, 3589.

38 S. D. Oladipo, R. C. Luckay, K. A. Olofinsan, A. A. Badeji and S. Mokoena, Exploring Schiff Bases Derived from 4-(Diethylamino) Salicylaldehyde and Their Copper(II) Complexes as Antidiabetes and Antioxidant Agents: Structural Elucidation, DFT Computational and in Vitro Studies, *Inorg. Chim. Acta*, 2025, **575**, 122447.

39 I. Waziri, T. L. Yusuf, H. A. Zarma, S. O. Oselusi, L.-C. C. Coetzee and A. S. Adeyinka, New Palladium(II) Complexes from Halogen Substituted Schiff Base Ligands: Synthesis, Spectroscopic, Biological Activity, Density Functional Theory, and Molecular Docking Investigations, *Inorg. Chim. Acta*, 2023, **552**, 121505.

40 S. Paul and P. Barman, Exploring Diaminomaleonitrile-Derived Schiff Base Ligand and Its Complexes: Synthesis, Characterization, Computational Insights, Biological Assessment, and Molecular Docking, *J. Mol. Struct.*, 2024, **1296**, 136941.

41 B. Samanta, J. Chakraborty, S. Shit, S. R. Batten, P. Jensen, J. D. Masuda and S. Mitra, Synthesis, Characterisation and Crystal Structures of a Few Coordination Complexes of Nickel(II), Cobalt(III) and Zinc(II) with *N*′-[(2-Pyridyl) Methylene] Salicyloylhydrazone Schiff Base, *Inorg. Chim. Acta*, 2007, **360**, 2471–2484.

42 D. Aggoun, M. Fernández-García, D. López, B. Bouzerafa, Y. Ouennoughi, F. Setifi and A. Ourari, New Nickel(II) and Copper(II) Bidentate Schiff Base Complexes, Derived from Dihalogenated Salicylaldehyde and Alkylamine: Synthesis, Spectroscopic, Thermogravimetry, Crystallographic Determination and Electrochemical Studies, *Polyhedron*, 2020, **187**, 114640.

43 J. Vakros, K. Bourikas, S. Perlepes, C. Kordulis and A. Lycourghiotis, Adsorption of Cobalt Ions on the "Electrolytic Solution/γ-Alumina" Interface Studied by Diffuse Reflectance Spectroscopy (DRS), *Langmuir*, 2004, **20**, 10542–10550, DOI: 10.1021/la048745w.

44 C. Bertucci and E. Domenici, Reversible and Covalent Binding of Drugs to Human Serum Albumin: Methodological Approaches and Physiological Relevance, *Curr. Med. Chem.*, 2002, **9**, 1463–1481.

45 G. Rabbani and S. N. Ahn, Roles of Human Serum Albumin in Prediction, Diagnoses and Treatment of COVID-19, *Int. J. Biol. Macromol.*, 2021, **193**, 948–955.

46 T. Bohnert and L.-S. Gan, Plasma Protein Binding: From Discovery to Development, *J. Pharm. Sci.*, 2013, **102**, 2953–2994.

47 O. K. Abou-Zied and O. I. K. Al-Shihi, Characterization of Subdomain IIA Binding Site of Human Serum Albumin in Its Native, Unfolded, and Refolded States Using Small Molecular Probes, *J. Am. Chem. Soc.*, 2008, **130**, 10793–10801, DOI: 10.1021/ja8031289.

48 S. Sookai and O. Q. Munro, Complexities of the Interaction of NiII, PdII and PtII Pyrrole-Imine Chelates with Human

Serum Albumin**, *ChemistryEurope*, 2023, **1**, e202300012, DOI: 10.1002/ceur.202300012.
49 S. Sookai, M. L. Bracken and M. Nowakowska, Spectroscopic and Computational pH Study of NiII and PdII Pyrrole-Imine Chelates with Human Serum Albumin, *Molecules*, 2023, **28**, 7466.
50 S.-S. Wu, W.-B. Yuan, H.-Y. Wang, Q. Zhang, M. Liu and K.-B. Yu, Synthesis, Crystal Structure and Interaction with DNA and HSA of (*N*,*N*′-Dibenzylethane-1,2-Diamine) Transition Metal Complexes, *J. Inorg. Biochem.*, 2008, **102**, 2026–2034.
51 S. Sookai, A. Majoka, M. A. Fernandes and M. Nowakowska, Binding Thermodynamics of 1,3-Bis(((*E*-1*H*-Pyrrol-2-Yl) Methylene) Amino) Propan-2-Ol Palladium(II) with HSA and Its Intercalative Behaviour in ctDNA, *J. Mol. Struct.*, 2025, 141880.
52 M. H. Gehlen, The Centenary of the Stern-Volmer Equation of Fluorescence Quenching: From the Single Line Plot to the SV Quenching Map, *J. Photochem. Photobiol., C*, 2020, **42**, 100338, DOI: 10.1016/j.jphotochemrev.2019.100338.
53 K. Flora, J. D. Brennan, G. A. Baker, M. A. Doody and F. V. Bright, Unfolding of Acrylodan-Labeled Human Serum Albumin Probed by Steady-State and Time-Resolved Fluorescence Methods, *Biophys. J.*, 1998, **75**, 1084–1096, DOI: 10.1016/S0006-3495(98)77598-8.
54 M. K. Helms, C. E. Petersen, N. V. Bhagavan and D. M. Jameson, Time-Resolved Fluorescence Studies on Site-Directed Mutants of Human Serum Albumin, *FEBS Lett.*, 1997, **408**, 67–70, DOI: 10.1016/S0014-5793(97)00389-X.
55 O. K. Abou-Zied and O. I. K. Al-Shihi, Characterization of Subdomain IIA Binding Site of Human Serum Albumin in Its Native, Unfolded, and Refolded States Using Small Molecular Probes, *J. Am. Chem. Soc.*, 2008, **130**, 10793–10801, DOI: 10.1021/ja8031289.
56 J. R. Lakowicz, *Principles of Fluorescence Spectroscopy*, Springer Science & Business Media, 2013; ISBN 978-1-4757-3061-6.
57 A. Hussain, M. F. AlAjmi, M. T. Rehman, S. Amir, F. M. Husain, A. Alsalme, M. A. Siddiqui, A. A. AlKhedhairy and R. A. Khan, Copper(II) Complexes as Potential Anticancer and Nonsteroidal Anti-Inflammatory Agents: In Vitro and in Vivo Studies, *Sci. Rep.*, 2019, **9**, 5237, DOI: 10.1038/s41598-019-41063-x.
58 M. Kumar, A. K. Singh, A. K. Singh, R. K. Yadav, S. Singh, A. P. Singh and A. Chauhan, Recent Advances in 3d-Block Metal Complexes with Bi, Tri, and Tetradentate Schiff Base Ligands Derived from Salicylaldehyde and Its Derivatives: Synthesis, Characterization and Applications, *Coord. Chem. Rev.*, 2023, **488**, 215176, DOI: 10.1016/j.ccr.2023.215176.
59 M. Dehkhodaei, M. Khorshidifard, H. Amiri Rudbari, M. Sahihi, G. Azimi, N. Habibi, S. Taheri, G. Bruno and R. Azadbakht, Synthesis, Characterization, Crystal Structure and DNA, HSA-Binding Studies of Four Schiff Base Complexes Derived from Salicylaldehyde and Isopropylamine, *Inorg. Chim. Acta*, 2017, **466**, 48–60, DOI: 10.1016/j.ica.2017.05.035.
60 M. van de Weert and C. Schönbeck, Ligand Binding to Proteins – When Flawed Fluorescence Quenching Methodology and Interpretation Become the New Norm, *Eur. J. Pharm. Sci.*, 2024, **203**, 106930, DOI: 10.1016/j.ejps.2024.106930.
61 I. Petitpas, A. A. Bhattacharya, S. Twine, M. East and S. Curry, Crystal Structure Analysis of Warfarin Binding to Human Serum Albumin: ANATOMY OF DRUG SITE I*, *J. Biol. Chem.*, 2001, **276**, 22804–22809, DOI: 10.1074/jbc.M100575200.
62 J. Ghuman, P. A. Zunszain, I. Petitpas, A. A. Bhattacharya, M. Otagiri and S. Curry, Structural Basis of the Drug-Binding Specificity of Human Serum Albumin, *J. Mol. Biol.*, 2005, **353**, 38–52, DOI: 10.1016/j.jmb.2005.07.075.
63 S. M. Kelly, T. J. Jess and N. C. Price, How to Study Proteins by Circular Dichroism, *Biochim. Biophys. Acta, Proteins Proteomics*, 2005, **1751**, 119–139, DOI: 10.1016/j.bbapap.2005.06.005.
64 X. M. He and D. C. Carter, Atomic Structure and Chemistry of Human Serum Albumin, *Nature*, 1992, **358**, 209–215, DOI: 10.1038/358209a0.
65 N. Sreerama and R. W. Woody, Computation and Analysis of Protein Circular Dichroism Spectra, *Methods in Enzymology*, Numerical Computer Methods, Part D, Academic Press, 2004, vol. 383, pp. 318–351.
66 Z. S. do Monte and C. S. Ramos, Development and Validation of a Method for the Analysis of Paroxetine HCl by Circular Dichroism, *Chirality*, 2013, **25**, 211–214, DOI: 10.1002/chir.22122.
67 X. M. He and D. C. Carter, Atomic Structure and Chemistry of Human Serum Albumin, *Nature*, 1992, **358**, 209–215, DOI: 10.1038/358209a0.
68 A. Micsonai, F. Wien, É. Bulyáki, J. Kun, É. Moussong, Y.-H. Lee, Y. Goto, M. Réfrégiers and J. Kardos, BeStSel: A Web Server for Accurate Protein Secondary Structure Prediction and Fold Recognition from the Circular Dichroism Spectra, *Nucleic Acids Res.*, 2018, **46**, W315–W322, DOI: 10.1093/nar/gky497.
69 F. Mohammadi, A.-K. Bordbar, A. Divsalar, K. Mohammadi and A. A. Saboury, Analysis of Binding Interaction of Curcumin and Diacetylcurcumin with Human and Bovine Serum Albumin Using Fluorescence and Circular Dichroism Spectroscopy, *Protein J.*, 2009, **28**, 189–196, DOI: 10.1007/s10930-009-9184-1.
70 H. A. Tajmir-Riahi, C. N. N'soukpoé-Kossi and D. Joly, Structural Analysis of Protein–DNA and Protein–RNA Interactions by FTIR, UV-Visible and CD Spectroscopic Methods, *Spectroscopy*, 2009, **23**, 81–101, DOI: 10.3233/SPE-2009-0371.
71 O. Duman, S. Tunç and B. Kancı Bozoğlan, Characterization of the Binding of Metoprolol Tartrate and Guaifenesin Drugs to Human Serum Albumin and Human Hemoglobin Proteins by Fluorescence and Circular Dichroism Spectroscopy, *J. Fluoresc.*, 2013, **23**, 659–669, DOI: 10.1007/s10895-013-1177-y.
72 P. Alam, S. K. Chaturvedi, T. Anwar, M. K. Siddiqi, M. R. Ajmal, G. Badr, M. H. Mahmoud and R. Hasan Khan, Biophysical and Molecular Docking Insight into the Interaction of Cytosine β-D Arabinofuranoside with Human Serum Albumin, *J. Lumin.*, 2015, **164**, 123–130, DOI: 10.1016/j.jlumin.2015.03.011.
73 D. Lafitte, P. O. Tsvetkov, F. Devred, R. Toci, F. Barras, C. Briand, A. A. Makarov and J. Haiech, Cation Binding

Mode of Fully Oxidised Calmodulin Explained by the Unfolding of the Apostate, *Biochim. Biophys. Acta, Proteins Proteomics*, 2002, **1600**, 105–110.

74 B. Ahmad, S. Parveen and R. H. Khan, Effect of Albumin Conformation on the Binding of Ciprofloxacin to Human Serum Albumin: A Novel Approach Directly Assigning Binding Site, *Biomacromolecules*, 2006, **7**, 1350–1356, DOI: 10.1021/bm050996b.

75 C. Sun, J. Yang, X. Wu, X. Huang, F. Wang and S. Liu, Unfolding and Refolding of Bovine Serum Albumin Induced by Cetylpyridinium Bromide, *Biophys. J.*, 2005, **88**, 3518–3524, DOI: 10.1529/biophysj.104.051516.

76 X.-X. Cheng, X.-Y. Fan, F.-L. Jiang, Y. Liu and K.-L. Lei, Resonance Energy Transfer, pH-Induced Folded States and the Molecular Interaction of Human Serum Albumin and Icariin, *Luminescence*, 2015, **30**, 1026–1033.

77 N. Zaidi, M. R. Ajmal, G. Rabbani, E. Ahmad and R. H. Khan, A Comprehensive Insight into Binding of Hippuric Acid to Human Serum Albumin: A Study to Uncover Its Impaired Elimination through Hemodialysis, *PLoS One*, 2013, **8**, e71422, DOI: 10.1371/journal.pone.0071422.

78 A. R. Leach, B. K. Shoichet and C. E. Peishoff, Prediction of Protein−Ligand Interactions. Docking and Scoring: Successes and Gaps, *J. Med. Chem.*, 2006, **49**, 5851–5855, DOI: 10.1021/jm060999m.

79 G. L. Warren, C. W. Andrews, A.-M. Capelli, B. Clarke, J. LaLonde, M. H. Lambert, M. Lindvall, N. Nevins, S. F. Semus and S. Senger, *et al.*, A Critical Assessment of Docking Programs and Scoring Functions, *J. Med. Chem.*, 2006, **49**, 5912–5931, DOI: 10.1021/jm050362n.

80 I. Petitpas, A. A. Bhattacharya, S. Twine, M. East and S. Curry, Crystal Structure Analysis of Warfarin Binding to Human Serum Albumin: ANATOMY OF DRUG SITE I*, *J. Biol. Chem.*, 2001, **276**, 22804–22809, DOI: 10.1074/jbc.M100575200.

81 J. C. Dabrowiak, *Metals in Medicine*, John Wiley & Sons, 2017.

82 A. R. Timerbaev, S. S. Aleksenko, K. Polec-Pawlak, R. Ruzik, O. Semenova, C. G. Hartinger, S. Oszwaldowski, M. Galanski, M. Jarosz and B. K. Keppler, Platinum Metallodrug-Protein Binding Studies by Capillary Electrophoresis-Inductively Coupled Plasma-Mass Spectrometry: Characterization of Interactions between Pt(II) Complexes and Human Serum Albumin, *Electrophoresis*, 2004, **25**, 1988–1995.

83 J. D. Holding, W. E. Lindup, D. A. Bowdler, M. Z. Siodlak and P. M. Stell, Disposition and Tumour Concentrations of Platinum in Hypoalbuminaemic Patients after Treatment with Cisplatin for Cancer of the Head and Neck, *Br. J. Clin. Pharmacol.*, 1991, **32**, 173–179.

84 C. Møller, H. S. Tastesen, B. Gammelgaard, I. H. Lambert and S. Stürup, Stability, Accumulation and Cytotoxicity of an Albumin-Cisplatin Adduct, *Metallomics*, 2010, **2**, 811–818.

85 J. E. Melvik, J. M. Dornish and E. O. Pettersen, The Binding of Cis-Dichlorodiammineplatinum(II) to Extracellular and Intracellular Compounds in Relation to Drug Uptake and Cytotoxicity in Vitro, *Br. J. Cancer*, 1992, **66**, 260–265.

86 J. A. Roberts, F. Pea and J. Lipman, The Clinical Relevance of Plasma Protein Binding Changes, *Clin. Pharmacokinet.*, 2013, **52**, 1–8, DOI: 10.1007/s40262-012-0018-5.

87 P. Gandia, S. Decheiver, M. Picard, R. Guilhaumou, S. Baklouti and D. Concordet, Hypoalbuminemia and Pharmacokinetics: When the Misunderstanding of a Fundamental Concept Leads to Repeated Errors over Decades, *Antibiotics*, 2023, **12**, 515, DOI: 10.3390/antibiotics12030515.

88 I. Waziri, S. Sookai, T. L. Yusuf, K. A. Olofinsan and A. J. Muller, Exploring Anticancer Activity and DNA Binding of Metal(II) Salicylaldehyde Schiff Base Complexes: A Convergence of Experimental and Computational Perspectives, *Appl. Organomet. Chem.*, 2025, **39**, e70162, DOI: 10.1002/aoc.70162.

89 J. Ghuman, P. A. Zunszain, I. Petitpas, A. A. Bhattacharya, M. Otagiri and S. Curry, Structural Basis of the Drug-Binding Specificity of Human Serum Albumin, *J. Mol. Biol.*, 2005, **353**, 38–52, DOI: 10.1016/j.jmb.2005.07.075.

90 E. Mullokandov, J. Ahn, A. Szalkiewicz and M. Babayeva, Protein Binding Drug-Drug Interaction between Warfarin and Tizoxanide in Human Plasma, *Austin J. Pharmacol. Ther.*, 2014, **2**(7), 3–7.

91 C. Dong, S. Ma and Y. Liu, Studies of the Interaction between Demeclocycline and Human Serum Albumin by Multi-Spectroscopic and Molecular Docking Methods, *Spectrochim. Acta, Part A*, 2013, **103**, 179–186, DOI: 10.1016/j.saa.2012.10.050.

92 A. Casini, Exploring the Mechanisms of Metal-Based Pharmacological Agents via an Integrated Approach, *J. Inorg. Biochem.*, 2012, **109**, 97–106, DOI: 10.1016/j.jinorgbio.2011.12.007.

